NREL
NATIONAL RENEWABLE ENERGY LABORATORY

BeamDyn: A High-Fidelity Wind Turbine Blade Solver in the FAST Modular Framework

Preprint

Q. Wang, M. Sprague, and J. Jonkman
National Renewable Energy Laboratory

N. Johnson
Colorado School of Mines

To be presented at SciTech 2015
Kissimmee, Florida
January 5–9, 2015

NREL is a national laboratory of the U.S. Department of Energy
Office of Energy Efficiency & Renewable Energy
Operated by the Alliance for Sustainable Energy, LLC

This report is available at no cost from the National Renewable Energy Laboratory (NREL) at www.nrel.gov/publications.

Conference Paper
NREL/CP-5000-63165
January 2015

Contract No. DE-AC36-08GO28308

NOTICE

This report is available at no cost from the National Renewable Energy Laboratory (NREL) at www.nrel.gov/publications.

Available electronically at http://www.osti.gov/scitech

Available for a processing fee to U.S. Department of Energy and its contractors, in paper, from:

U.S. Department of Energy
Office of Scientific and Technical Information
P.O. Box 62
Oak Ridge, TN 37831-0062
phone: 865.576.8401
fax: 865.576.5728
email: mailto:reports@adonis.osti.gov

Available for sale to the public, in paper, from:

U.S. Department of Commerce
National Technical Information Service
5285 Port Royal Road
Springfield, VA 22161
phone: 800.553.6847
fax: 703.605.6900
email: orders@ntis.fedworld.gov
online ordering: http://www.ntis.gov/help/ordermethods.aspx

Cover Photos: (left to right) photo by Pat Corkery, NREL 16416, photo from SunEdison, NREL 17423, photo by Pat Corkery, NREL 16560, photo by Dennis Schroeder, NREL 17613, photo by Dean Armstrong, NREL 17436, photo by Pat Corkery, NREL 17721.

BeamDyn: A High-Fidelity Wind Turbine Blade Solver in the FAST Modular Framework

Qi Wang*[1], Nick Johnson†[2], Michael A. Sprague‡[1], and Jason Jonkman§[1]

[1]National Renewable Energy Laboratory, Golden, CO 80401
[2]Colorado School of Mines, Golden, CO 80401

BeamDyn, a Legendre-spectral-finite-element implementation of geometrically exact beam theory (GEBT), was developed to meet the design challenges associated with highly flexible composite wind turbine blades. In this paper, the governing equations of GEBT are reformulated into a nonlinear state-space form to support its coupling within the modular framework of the FAST wind turbine computer-aided engineering (CAE) tool. Different time integration schemes (implicit and explicit) were implemented and examined for wind turbine analysis. Numerical examples are presented to demonstrate the capability of this new beam solver. An example analysis of a realistic wind turbine blade, the CX-100, is also presented as validation.

I. Introduction

In recent years, wind power installations in the United States have exceeded 60 gigawatts in generation capacity, and have become an increasingly important part of the overall energy portfolio. Simultaneously, the size of wind turbines has also increased in the quest for economies of scale. To ensure the performance and reliability of wind turbines, it is crucial to use computer-aided engineering (CAE) tools that are capable of analyzing wind turbine blades accurately and efficiently. Although modern computers enable three-dimensional (3D) analysis of a fully resolved blade, such analyses are too expensive for iterative and probabilistic design. However, composite wind turbine blades are well represented as nonlinear beam models, which can capture the deformation response under realistic operating conditions with high fidelity, and in a small fraction of the time required by a fully resolved 3D simulation.

Beam models are widely used to analyze structures in which one dimension is much larger than the other two. Many engineering structures such as bridges, joists, and helicopter rotor blades may be modeled as beams. Similarly, beam models are well suited for analyzing wind turbine blades, towers, and shafts. Most wind turbine blades are constructed of composite materials, which are more complicated than isotropic beams to analyze because of elastic coupling effects, high flexibility, and initial twist/curvatures. The geometrically exact beam theory (GEBT), first proposed by Reissner[1], is a beam-deformation model useful in efficient analysis of highly flexible composite structures. For instance, GEBT has demonstrated efficacy in helicopter rotor analysis[2]. Simo[3] and Simo and Vu-Quoc[4] extended Reissner's work to include 3D dynamic problems. Jelenić and Crisfield[5] derived a finite-element (FE) method that interpolates the rotation field, thereby preserving the geometric exactness of this theory. Notably, Ibrahimbegović and his colleagues implemented this theory for static[6] and dynamic[7] analysis. Readers are referred to Hodges[8], in which comprehensive derivations and discussions on nonlinear composite-beam theories can be found. Recently, a mixed FE formulation of GEBT along with the numerical implementation was presented by Yu and Blair[9].

FAST is a CAE tool developed by the National Renewable Energy Laboratory (NREL) for analyzing both land-based and offshore wind turbines under realistic operating conditions. The current beam model in FAST is not capable of predictive analysis of highly flexible, composite wind turbine blades. Recently, FAST has been reformulated under a new modularized framework that provides a rigorous means by which various mathematical systems are implemented in distinct modules. These modules are interconnected to solve for the globally coupled dynamic responses of wind turbines and wind plants[10,11].

In this paper, a 3D displacement-based implementation of geometrically exact beam theory using Legendre spectral finite elements is presented. The theory is reformulated in a nonlinear state-space form for the purpose of integrating with the FAST framework, thereby introducing an optional high-fidelity beam model as an alternative to the current beam model. Several first-order form time integrators, including the explicit fourth-order Runge-Kutta (RK4) and implicit second-order Adams-Moulton (AM2), are examined. This work builds on previous efforts that demonstrated the implementation of GEBT and spatial discretization using Legendre spectral finite elements (LSFEs)[12–15] in analyzing

*Research Engineer, National Wind Technology Center, AIAA Member. Email: Qi.Wang2@nrel.gov
†Graduate Research Assistant, Department of Mechanical Engineering.
‡Senior Research Scientist, Computational Science Center.
§Senior Engineer, National Wind Technology Center, AIAA Professional Member.

composite wind turbine blades. The paper is organized as follows. First, the theoretical foundation of the geometrically exact beam theory along with the reformulation of the governing equations into a state-space form is introduced. Coupling to the FAST framework is then discussed. Finally, numerical examples are provided to verify and validate the accuracy and efficiency of the present model for composite wind turbine blades.

II. Geometrically Exact Beam Theory

This section briefly reviews the geometrically exact beam theory. Further details on the content of this section can be found in many other papers and textbooks[8,9,16]. Figure 1 shows a beam in its initial undeformed and deformed states. A reference frame $\mathbf{b}_i$ is introduced along the beam axis for the undeformed state and a frame $\mathbf{B}_i$ is introduced along each point of the deformed beam axis. The curvilinear coordinate x_1 defines the intrinsic parameterization of the reference line. In this paper, matrix notation is used to denote vectorial or vectorial-like quantities. For example,

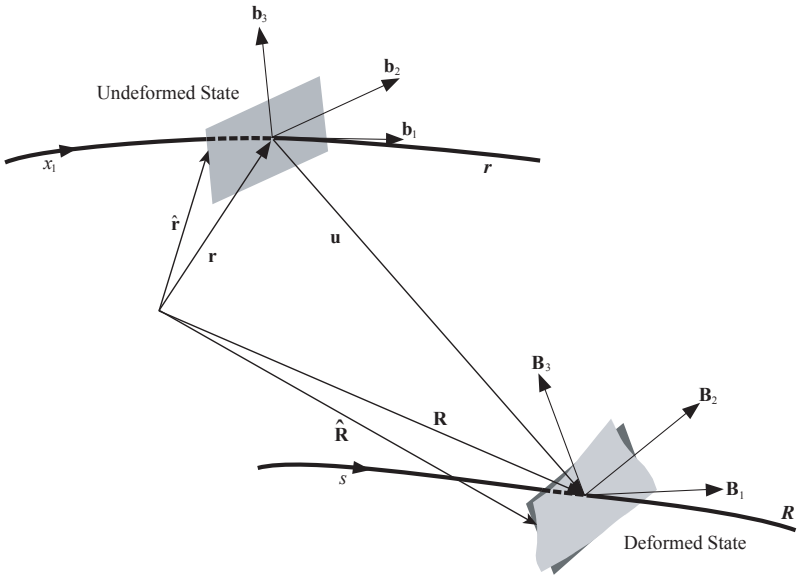

Figure 1: A beam deformation schematic.

an underline denotes a vector $\underline{u}$, a bar denotes unit vector $\bar{n}$, and a double underline denotes a tensor $\underline{\underline{\Delta}}$. Note that sometimes the underlines only denote the dimension of the corresponding matrix. The governing equations of motion for geometrically exact beam theory can be written as[16]

$$\underline{\dot{h}} - \underline{F}' = \underline{f} \tag{1}$$

$$\underline{\dot{g}} + \tilde{\dot{u}}\underline{h} - \underline{M}' + (\tilde{x}_0' + \tilde{u}')^T \underline{F} = \underline{m} \tag{2}$$

where $\underline{h}$ and $\underline{g}$ are the linear and angular momenta resolved in the inertial coordinate system, respectively; $\underline{F}$ and $\underline{M}$ are the beam's sectional force and moment resultants, respectively; $\underline{u}$ is the one-dimensional (1D) displacement of a point on the reference line; $\underline{x}_0$ is the position vector of a point along the beam's reference line; and $\underline{f}$ and $\underline{m}$ are the distributed force and moment applied to the beam structure. The notation $(\bullet)'$ indicates a derivative with respect to beam axis x_1 and $(\dot{\bullet})$ indicates a derivative with respect to time. The tilde operator $(\widetilde{\bullet})$ defines a skew-symmetric tensor corresponding to the given vector. In the literature, it is also termed as "cross-product matrix". For example,

$$\widetilde{n} = \begin{bmatrix} 0 & -n_3 & n_2 \\ n_3 & 0 & -n_1 \\ -n_2 & n_1 & 0 \end{bmatrix}$$

The constitutive equations relate the velocities to the momenta and the 1D strain measures to the sectional resultants as

$$\begin{Bmatrix} \underline{h} \\ \underline{g} \end{Bmatrix} = \underline{\underline{\mathcal{M}}} \begin{Bmatrix} \underline{\dot{u}} \\ \underline{\omega} \end{Bmatrix} \tag{3}$$

$$\begin{Bmatrix} \underline{F} \\ \underline{M} \end{Bmatrix} = \underline{\underline{\mathcal{C}}} \begin{Bmatrix} \underline{\epsilon} \\ \underline{\kappa} \end{Bmatrix} \tag{4}$$

where $\underline{\underline{\mathcal{M}}}$ and $\underline{\underline{\mathcal{C}}}$ are the 6×6 sectional mass and stiffness matrices, respectively (note that they are not really tensors); $\underline{\epsilon}$ and $\underline{\kappa}$ are the 1D strains and curvatures, respectively; and, $\underline{\omega}$ is the angular velocity vector that is defined by the rotation tensor $\underline{\underline{R}}$ as $\underline{\omega} = axial(\dot{\underline{\underline{R}}}\,\underline{\underline{R}}^T)$. The axial vector $\underline{a}$ associated with a second-order tensor $\underline{\underline{A}}$ is denoted $\underline{a} = axial(\underline{\underline{A}})$ and its components are defined as

$$\underline{a} = axial(\underline{\underline{A}}) = \begin{Bmatrix} a_1 \\ a_2 \\ a_3 \end{Bmatrix} = \frac{1}{2}\begin{Bmatrix} A_{32} - A_{23} \\ A_{13} - A_{31} \\ A_{21} - A_{12} \end{Bmatrix} \tag{5}$$

The 1D strain measures are defined as

$$\begin{Bmatrix} \underline{\epsilon} \\ \underline{\kappa} \end{Bmatrix} = \begin{Bmatrix} \underline{x}_0' + \underline{u}' - (\underline{\underline{R}}\,\underline{\underline{R}}_0)\bar{\imath}_1 \\ \underline{k} \end{Bmatrix} \tag{6}$$

where $\underline{k} = axial[(\underline{\underline{RR_0}})'(\underline{\underline{RR_0}})^T]$ is the sectional curvature vector resolved in the inertial basis and $\bar{\imath}_1$ is the unit vector along x_1 direction in the inertial basis. Note that these three sets of equations, including equations of motion Eq. (1) and (2), constitutive equations Eq. (3) and (4), and kinematical equations Eq. (6), provide a full mathematical description of elasticity problems.

For a displacement-based finite-element implementation, there are six degrees of freedom at each node: three displacement components and three rotation components. Here, $\underline{q}$ denotes the elemental displacement array as $\underline{q}^T = \begin{bmatrix}\underline{u}^T & \underline{p}^T\end{bmatrix}$ where $\underline{u}$ is the displacement and $\underline{p}$ is the rotation-parameter vector. The acceleration array can thus be defined as $\underline{a}^T = \begin{bmatrix}\ddot{\underline{u}}^T & \dot{\underline{\omega}}^T\end{bmatrix}$. For nonlinear finite-element analysis, the discretized forms of displacement, velocity, and acceleration are written as

$$\underline{q}(x_1) = \underline{\underline{N}}\,\hat{\underline{q}} \qquad \underline{q}^T = \begin{bmatrix}\underline{u}^T & \underline{p}^T\end{bmatrix} \tag{7}$$

$$\underline{v}(x_1) = \underline{\underline{N}}\,\hat{\underline{v}} \qquad \underline{v}^T = \begin{bmatrix}\dot{\underline{u}}^T & \underline{\omega}^T\end{bmatrix} \tag{8}$$

$$\underline{a}(x_1) = \underline{\underline{N}}\,\hat{\underline{a}} \qquad \underline{a}^T = \begin{bmatrix}\ddot{\underline{u}}^T & \dot{\underline{\omega}}^T\end{bmatrix} \tag{9}$$

where $\underline{\underline{N}}$ is the shape function matrix and $\hat{(\cdot)}$ denotes a column matrix of nodal values.

III. State-Space Formulation

NREL has put considerable effort into improving the modularity of FAST. The modules in the new framework can be coupled in one of two ways in the time domain: loose and tight. In the loose coupling scheme, data are exchanged between the modules at each coupling step, but each module tracks its own states and integrates its own equations with its own solver. In a tightly coupled time-integration scheme, each module sets up its own equations, but the states are tracked and integrated by a solver common to all of the modules. To enable the most flexibility, it is useful to create modules (such as BeamDyn) so that they can support both loose and tight coupling. More details on the FAST modularization framework and an initial assessment of the numerical stability, numerical accuracy, and computational performance of various coupling schemes can be found in [10,15,17].

To accommodate the tight coupling scheme in the FAST modular framework, the governing equations (1) and (2) needed to be reformulated into a state-space form. First, these equations are recast in compact form as

$$\underline{\mathcal{F}}^I - (\underline{\mathcal{F}}^C)' + \underline{\mathcal{F}}^D = \underline{\mathcal{F}}^{ext} \tag{10}$$

where $\underline{\mathcal{F}}^I$, $\underline{\mathcal{F}}^C$ and $\underline{\mathcal{F}}^D$, and $\underline{\mathcal{F}}^{ext}$ are the inertial force term, two elastic force terms, and externally applied force term, respectively; their definitions are

$$\underline{\mathcal{F}}^I = \begin{Bmatrix}\dot{\underline{h}} \\ \dot{\underline{g}}\end{Bmatrix} + \begin{bmatrix}\underline{\underline{0}} & \underline{\underline{0}} \\ \tilde{\underline{u}} & \underline{\underline{0}}\end{bmatrix}\begin{Bmatrix}\underline{h} \\ \underline{g}\end{Bmatrix} \tag{11}$$

$$\underline{\mathcal{F}}^C = \begin{Bmatrix}\underline{F} \\ \underline{M}\end{Bmatrix} \tag{12}$$

$$\underline{\mathcal{F}}^D = \begin{Bmatrix}\underline{0} \\ (\tilde{x}_0' + \tilde{u}')^T\underline{F}\end{Bmatrix} \tag{13}$$

$$\underline{\mathcal{F}}^{ext} = \begin{Bmatrix}\underline{f} \\ \underline{m}\end{Bmatrix} \tag{14}$$

Along with the constitutive equations (3) and (4), the inertial force $\underline{\mathcal{F}}^I$ can be written explicitly as

$$\begin{aligned}\underline{\mathcal{F}}^I &= \begin{Bmatrix} m\underline{\ddot{u}} + (\dot{\tilde{\omega}} + \tilde{\omega}\tilde{\omega})m\underline{\eta} \\ m\tilde{\eta}\underline{\ddot{u}} + \underline{\underline{\varrho}}\,\underline{\dot{\omega}} + \tilde{\omega}\underline{\underline{\varrho}}\,\underline{\omega} \end{Bmatrix} \\ &= \begin{bmatrix} m\underline{\underline{I}} & m\tilde{\eta}^T \\ m\tilde{\eta} & \underline{\underline{\varrho}} \end{bmatrix} \begin{Bmatrix} \underline{\ddot{u}} \\ \underline{\dot{\omega}} \end{Bmatrix} + \begin{bmatrix} \underline{\underline{0}} & m\tilde{\omega}\tilde{\eta}^T \\ \underline{\underline{0}} & \tilde{\omega}\underline{\underline{\varrho}} \end{bmatrix} \begin{Bmatrix} \underline{\dot{u}} \\ \underline{\omega} \end{Bmatrix} \\ &\equiv \underline{\underline{\mathfrak{M}}}\,\underline{a} + \underline{\underline{\mathcal{G}}}\,\underline{v} \end{aligned} \tag{15}$$

where m is the mass density per unit span; $\underline{\eta}$ is the center of mass location; $\underline{\underline{\varrho}}$ is the moment of inertia; and $\underline{\underline{I}}$ is the identity matrix. The definitions of the acceleration vector $\underline{a}$ and velocity vector $\underline{v}$ can be found in Eq. (9) and (8), respectively. Using the newly introduced matrices, the compact form of the equations of motion can be rewritten as

$$\underline{\underline{\mathfrak{M}}}\,\underline{a} + f(\underline{q}, \underline{v}, t) = 0 \tag{16}$$

where

$$f(\underline{q}, \underline{v}, t) = \underline{\mathcal{F}}^F - \underline{\mathcal{F}}^{C\prime} + \underline{\mathcal{F}}^D - \underline{\mathcal{F}}^{ext} \tag{17}$$

$$\begin{aligned}\underline{\mathcal{F}}^F &= \underline{\underline{\mathcal{G}}}\,\underline{v} \\ &= \begin{bmatrix} \underline{\underline{0}} & m\tilde{\omega}\tilde{\eta}^T \\ \underline{\underline{0}} & \tilde{\omega}\underline{\underline{\varrho}} \end{bmatrix} \begin{Bmatrix} \underline{\dot{u}} \\ \underline{\omega} \end{Bmatrix} \end{aligned} \tag{18}$$

A weighted residual formulation is used to enforce the dynamic equilibrium conditions in Eq. (16)

$$\int_0^l \underline{\underline{N}}^T(\underline{\underline{\mathfrak{M}}}\,\underline{a} + \underline{\mathcal{F}}^F - \underline{\mathcal{F}}^{C\prime} + \underline{\mathcal{F}}^D - \underline{\mathcal{F}}^{ext})dx_1 = 0 \tag{19}$$

The above equation can be recast as

$$\underline{\underline{M}}\,\hat{a} = F(\underline{q}, \underline{v}, t) \tag{20}$$

where

$$\underline{\underline{M}} = \int_0^l \underline{\underline{N}}^T \underline{\underline{\mathfrak{M}}}\,\underline{\underline{N}}\,dx_1 \tag{21}$$

$$\underline{F}(\underline{q}, \underline{v}, t) = \int_0^l \underline{\underline{N}}^T(-\underline{\mathcal{F}}^F + \underline{\mathcal{F}}^{C\prime} - \underline{\mathcal{F}}^D + \underline{\mathcal{F}}^{ext})dx_1 \tag{22}$$

To derive the state-space form of the governing equations, the state variable in first-order form $\underline{x}(t)$ is introduced as

$$\underline{x}(t) \equiv \begin{Bmatrix} \underline{q}(t) \\ \underline{v}(t) \end{Bmatrix} \tag{23}$$

Note that the second component of $\underline{x}(t)$ is not $\dot{\underline{q}}$ but $\underline{v}$ because the angular velocity $\underline{\omega}$ cannot be calculated as the time derivative of the rotation parameter $\underline{p}$. The angular velocity is related to the rotation parameter by the tangent matrix as $\omega = \underline{\underline{H}}(p)\dot{\underline{p}}$[16]. Substituting the discretized quantities in Eqs. (7) to (9) into Eq. (23) and using the relation

$$\underline{a} = \dot{\underline{v}} = \begin{Bmatrix} \underline{\ddot{u}} \\ \underline{\dot{\omega}} \end{Bmatrix} \tag{24}$$

The state-space form can be obtained as

$$\underline{\underline{A}}\,\dot{\underline{\hat{x}}}(t) = \mathfrak{f}(\underline{\hat{x}}(t), t) \tag{25}$$

with initial condition

$$\underline{\hat{x}}(0) = \underline{\hat{x}}_0 \tag{26}$$

where

$$\underline{\underline{A}}(\underline{\hat{x}}(t)) = \begin{matrix} \underline{\underline{D}} & \underline{\underline{0}} \\ \underline{\underline{0}} & \underline{\underline{M}} \end{matrix} \tag{27}$$

$$\underline{\underline{D}}(\underline{\hat{x}}(t)) = \int_0^l \underline{\underline{N}}^T \begin{matrix} \underline{\underline{I}}_3 & \underline{\underline{0}} \\ \underline{\underline{0}} & \underline{\underline{H}} \end{matrix} \underline{\underline{N}}\,dx_1 \tag{28}$$

$$\mathfrak{f}(\underline{\hat{x}}(t), t) = \begin{Bmatrix} \int_0^l \underline{\underline{N}}^T \underline{v}\,dx_1 \\ \underline{F}(\underline{\hat{x}}(t), t) \end{Bmatrix} \tag{29}$$

$$\underline{\hat{x}}_0 = \begin{Bmatrix} \underline{\hat{q}}_0 \\ \underline{\hat{v}}_0 \end{Bmatrix} \tag{30}$$

Note that the state-space form, in Eq. (25) and (26), can be solved with any number of ordinary differential equations (ODE) integrators for first-order-in-time systems. A viscous damping term is also implemented to account for the structural damping. The damping force is defined as

$$\underline{f}_d = \underline{\underline{\mu}}\,\underline{\underline{\mathcal{C}}} \begin{Bmatrix} \dot{\epsilon} \\ \dot{\kappa} \end{Bmatrix} \tag{31}$$

where $\underline{\underline{\mu}}$ is a user-provided damping-coefficient diagonal matrix. The damping force can be recast in two separate parts, like $\underline{\mathcal{F}}^C$ and $\underline{\mathcal{F}}^D$ in the elastic force, as

$$\underline{\mathcal{F}}_d^C = \begin{Bmatrix} \underline{F}_d \\ \underline{M}_d \end{Bmatrix} \tag{32}$$

$$\underline{\mathcal{F}}_d^D = \begin{Bmatrix} \underline{0} \\ (\tilde{x}_0' + \tilde{u}')^T \underline{F}_d \end{Bmatrix} \tag{33}$$

Readers are refered to Ref.[16] for more details on the damping force and its linearization.

IV. Implementation of BeamDyn

The state-space form of GEBT was numerically implemented into a beam solver, called BeamDyn. BeamDyn has two sources of input: the user-prescribed parameters and per time step data from the FAST driver code. The input parameters from the users are:

1. Key points that define the natural geometry of the beam; these key points are interpolated by cubic splines
2. Sectional constants for a 1D beam model
3. Finite-element mesh information (order of element)
4. Selection of static[14] or dynamic analysis
5. Time integrators and associated parameters: RK4, AM2, or Generalized-α (for loosing coupling only).

It is intended to couple separate instances of BeamDyn to FAST for each blade. Structurally, the coupling will involve passing motions of the blade root for each blade from FAST's ElastoDyn structural module to BeamDyn; including position, velocity, and acceleration (both translation and rotation); and passing root loads for each blade from BeamDyn to ElastoDyn (both forces and moments). Aerodynamically, the coupling will involve passing motions of the nodes distributed along each blade from BeamDyn to FAST's AeroDyn aerodynamics module; including position, velocity, and acceleration (both translation and rotation); and passing aerodynamic loads distributed along the blade from AeroDyn to BeamDyn. FAST will also send BeamDyn the gravity vector and initial hub motions at initialization to enable an initialization of BeamDyn's states. While not needed to enable the coupling of BeamDyn to FAST, BeamDyn will also calculate the internal loads along the beam, calculated by subtracting the inertial loads from the externally applied loads.

The implementation of GEBT with RK4 is straightforward; however, for the AM2 scheme, a linearization is required because of its implicit nature. By applying the trapezoidal rule, the state-space form in Eq. (25) can be recast as

$$\underline{\underline{A}}_{k+1}(\hat{\underline{x}}_{k+1} - \hat{\underline{x}}_k - \frac{\Delta t}{2}\dot{\hat{\underline{x}}}_k) = \frac{\Delta t}{2}\mathfrak{f}(\hat{\underline{x}}_{k+1}, t_{k+1}) \tag{34}$$

where the subscript denotes the discretized time step in which the value is evaluated, and Δt is the time step size. A linearization is needed to solve this nonlinear equation. The linearized equation is as follows

$$\begin{matrix} \hat{\underline{\underline{K}}}_1 & \hat{\underline{\underline{C}}}_1 \\ \hat{\underline{\underline{K}}}_2 & \hat{\underline{\underline{C}}}_2 \end{matrix} \begin{Bmatrix} \Delta\hat{\underline{q}} \\ \Delta\hat{\underline{v}} \end{Bmatrix} = \begin{Bmatrix} \hat{\underline{F}}_1 \\ \hat{\underline{F}}_2 \end{Bmatrix} \tag{35}$$

The coefficient matrices are written as

$$\underline{\underline{\hat{K}}}_1 = \int_0^l \underline{\underline{N}}^T \underline{\underline{K}}_1 \underline{\underline{N}}\, dx_1 \tag{36}$$

$$\underline{\underline{\hat{C}}}_1 = \int_0^l \underline{\underline{N}}^T \underline{\underline{C}}_1 \underline{\underline{N}}\, dx_1 \tag{37}$$

$$\begin{aligned}\underline{\underline{\hat{K}}}_2 = &\int_0^l \underline{\underline{N}}^T (\underline{\underline{A}}_2 - \underline{\underline{A}}_3 + \frac{\Delta t}{2}\underline{\underline{A}}_1 + \frac{\Delta t}{2}\underline{\underline{A}}_5 + \frac{\Delta t}{2}\mathcal{Q})\underline{\underline{N}}\, dx_1 \\ &+ \int_0^l \left(\underline{\underline{N}}^T \frac{\Delta t}{2}\underline{\underline{\mathcal{P}}}\,\underline{\underline{N}}' + \underline{\underline{N}}'^T \frac{\Delta t}{2}\underline{\underline{\mathcal{S}}}\,\underline{\underline{N}}' + \underline{\underline{N}}^T \frac{\Delta t}{2}\underline{\underline{\mathcal{O}}}\,\underline{\underline{N}}\right) dx_1\end{aligned} \tag{38}$$

$$\underline{\underline{\hat{C}}}_2 = \int_0^l \underline{\underline{N}}^T (\underline{\underline{\mathfrak{M}}} + \frac{\Delta t}{2}\underline{\underline{A}}_4)\,\underline{\underline{N}}\, dx_1 \tag{39}$$

where the newly introduced matrices are

$$\underline{\underline{K}}_1 = \begin{matrix}\underline{\underline{I}}_3 & \underline{\underline{0}} \\ \underline{\underline{0}} & \underline{\underline{B}}(\underline{p},\underline{p}) + \underline{\underline{H}} - \underline{\underline{B}}(\underline{p},\underline{p}_k) - \frac{\Delta t}{2}\underline{\underline{B}}(\underline{p},\dot{\underline{p}}_k)\end{matrix} \tag{40}$$

$$\underline{\underline{C}}_1 = -\frac{\Delta t}{2}\begin{matrix}\underline{\underline{I}}_3 & \underline{\underline{0}} \\ \underline{\underline{0}} & \underline{\underline{I}}_3\end{matrix} \tag{41}$$

$$\underline{\underline{A}}_1 = \begin{matrix}\underline{\underline{0}} & m\dot{\tilde{\omega}}_k\tilde{\eta}^T \\ \underline{\underline{0}} & m\ddot{\tilde{u}}_k\tilde{\eta} + \underline{\underline{\rho}}\dot{\tilde{\omega}}_k - \widetilde{\underline{\underline{\rho}}\underline{\omega}_k}\end{matrix} \tag{42}$$

$$\underline{\underline{A}}_2 = \begin{matrix}\underline{\underline{0}} & m\tilde{\omega}\tilde{\eta}^T \\ \underline{\underline{0}} & m\dot{\tilde{u}}\tilde{\eta} + \underline{\underline{\rho}}\tilde{\omega} - \widetilde{\underline{\underline{\rho}}\underline{\omega}}\end{matrix} \tag{43}$$

$$\underline{\underline{A}}_3 = \begin{matrix}\underline{\underline{0}} & m\tilde{\omega}_k\tilde{\eta}^T \\ \underline{\underline{0}} & m\dot{\tilde{u}}_k\tilde{\eta} + \underline{\underline{\rho}}\tilde{\omega}_k - \widetilde{\underline{\underline{\rho}}\underline{\omega}_k}\end{matrix} \tag{44}$$

$$\underline{\underline{A}}_4 = \begin{matrix}\underline{\underline{0}} & \widetilde{\tilde{\omega}m\underline{\eta}}^T + \tilde{\omega}m\tilde{\eta}^T \\ \underline{\underline{0}} & \widetilde{\underline{\underline{\rho}}\underline{\omega}}^T + \tilde{\omega}\underline{\underline{\rho}}\end{matrix} \tag{45}$$

$$\underline{\underline{A}}_5 = \begin{matrix}\underline{\underline{0}} & \tilde{\omega}\tilde{\omega}m\tilde{\eta}^T \\ \underline{\underline{0}} & \tilde{\omega}(\underline{\underline{\rho}}\tilde{\omega} - \widetilde{\underline{\underline{\rho}}\underline{\omega}}\end{matrix} \tag{46}$$

The $\underline{\underline{\mathcal{O}}}$, $\underline{\underline{\mathcal{P}}}$, $\underline{\underline{\mathcal{Q}}}$, and $\underline{\underline{\mathcal{S}}}$ can be found in previous work by Wang et al[14]. It is also noted that the $\underline{\underline{B}}$ matrix is a linearization of the tangent matrix $\underline{\underline{H}}$ defined as

$$\underline{\underline{B}}(\underline{p},\underline{a}) = \frac{\partial(\underline{\underline{H}}(\underline{p}))\underline{a}}{\partial \underline{p}} \tag{47}$$

One major difficulty in implementing geometrically nonlinear theory is the description of rotations in 3D space. As discussed in many articles[16,18,19], there will be a singular point for any type of vectorial parameterization. To address this singular point, we implemented an algorithm proposed by Crisfield and Jelenić[18], in which the relative rotations are interpolated instead of the total rotations within one element. Although the magnitude of the total rotation may be large, it is reasonable to assume that the relative rotation in one finite element is smaller than π. In the time domain, all the nodal rotations need to be rescaled at the same time so the highly nonlinear governing equations in Eq. (1) and (2) are linearized about the correct point.

In summary, the newly developed BeamDyn has the following features:

1. It is based on the state-space form of geometrically exact beam theory, thus, it can be easily integrated into FAST as a structural module with both loose-coupling and tight-coupling schemes using time integrators for first-order form ordinary differential equations (ODEs)

2. The spectral finite-element method is used to discretize the space domain; exponential convergence rate can be expected for a smooth solution

3. It is compatible with the FAST modularization network. Variables are categorized into input, output, states, and parameters.

V. BeamDyn Verification and Validation

In this section, several numerical cases to verify and validate BeamDyn against numerical solutions and experimental data are presented. As discussed in the introduction, modern wind turbine blade features include initial twists/curvatures, elastic coupling, and high flexibility. BeamDyn's capabilities in addressing these features are examined.

A. Initially Twisted/Curved Beams

An initially twisted beam was examined first. A straight beam ($k_2 = k_3 = 0$) with an initial twist ($k_1 \neq 0$) is shown in Figure 2. The beam is linearly twisted in the positive θ_1 direction from 0 degrees at the root to 90 degrees at the tip. Table 1 shows the material properties for A36 steel, the beam geometry, and the force applied at the free tip along x_3 direction. The height and base values reported in the table are the height and base of the rectangular cross section. The beam was discretized using a seventh-order LSFE to obtain a converged results. It is widely known that the well-refined 3D finite-element solution can be considered exact; here we use the 3D results as benchmark solutions. The results for the twisted beam are shown in Table 2 and compared to the baseline results obtained from extremely refined 3D ANSYS analysis using SOLID186 elements. We see that the tip results are quite large (35% of total length) and that the agreement between the solid-element and beam-element solutions is very good. These results also serve to validate the beam-modeling approach.

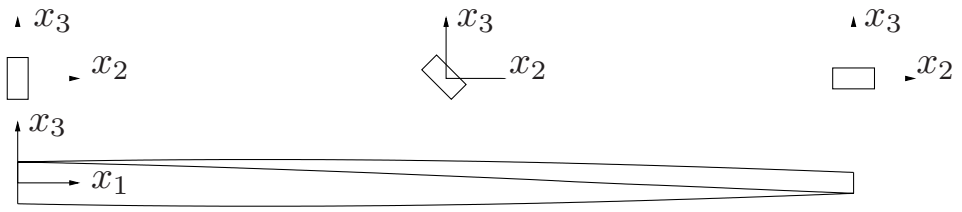

Figure 2: Sketch of an initially twisted beam.

Table 1: Properties of twisted beam

Property	Value
Elastic Modulus	200 GPa
Shear Modulus	79.3 GPa
Height	0.5 m
Base	0.25 m
Length	10 m
Force	4000 kN

Table 2: Comparison of tip displacements of an initially twisted beam

	u_1 (m)	u_2 (m)	u_3 (m)
BeamDyn	-1.132727	-1.715123	-3.578671
ANSYS	-1.134192	-1.714467	-3.584232
Percent Error	0.129%	0.038%	0.155%

Next, an initially curved beam was examined. It is clear that the initial curvature plays a major role in the distribution of the elastic forces within the beam. As such, it is very important to ensure that BeamDyn is capable of modeling this effect properly. A widely used benchmark problem for a curved beam is the case proposed by Bathe[20], which was analyzed for verification. Figure 3 shows the configuration of the cantilevered curved beam being analyzed. The beam lies in the x_1, x_2 plane, the positive x_1 direction and the negative x_2 direction. A force of 600 pounds is applied in the positive x_3 direction. The beam is defined by the 45-degree arc with 100-inch radius centered at 100 inches in the negative x_2 direction. The geometry of the cross section for the curved beam is square, and the material properties can

be found in Ref.[20]. The beam was discretized by a fifth-order LSFE. The results of this static analysis are shown in Table 3 and are compared to the results published in Bathe[20].

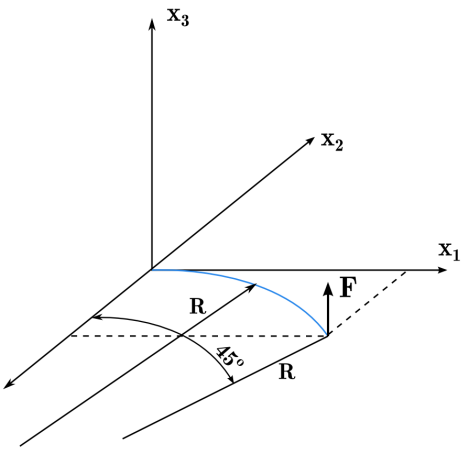

Figure 3: Sketch of an initially curved beam.

Table 3: Comparison of tip displacements of an initially curved beam

	u_1 (inches)	u_2 (inches)	u_3 (inches)
BeamDyn (one LSFE)	-23.7	13.5	53.4
Bathe-Bolourchi[20]	-23.5	13.4	53.4

It can be seen from these results that the simulations from BeamDyn for a initially curved beam match quite well with the published results. The results of these cases suggest that BeamDyn is capable of modeling beams with initial twist and curvatures.

B. Static Analysis of CX-100 Blade

The primary intended use of BeamDyn is analyzing anisotropic wind turbine blades, therefore, the CX-100 was chosen as a validation case. The CX-100 is a 9-m blade designed by Sandia National Laboratories[21]. It was chosen for this analysis because it is well characterized, with a wealth of publicly available data regarding its construction and material properties.

The cross-sectional properties as derived from VABS for this beam were provided by D.J. Luscher of Los Alamos National Laboratory. These properties were provided at 40 points along the beam. For example, a typical stiffness matrix corresponding to 2.2 m along the span of the blade is given by

$$C = 10^3 \times \begin{bmatrix} 193,000 & -75.4 & 12.2 & -75.2 & -1970 & -3500 \\ -75.4 & 19,500 & 4,760 & 62.6 & 67.3 & 11.3 \\ 12.2 & 4,760 & 7,210 & -450 & 17.0 & 2.68 \\ -75.2 & 62.6 & -450 & 518 & 1.66 & -1.11 \\ -1,970 & 67.3 & 17.0 & 1.66 & 2,280 & -879 \\ -3,500 & 11.6 & 2.68 & -1.11 & -875 & 4,240 \end{bmatrix}$$

where the units associated with stiffness values are C_{ij} (N), $C_{i,j+3}$ (N $\cdot$ m), and $C_{i+3,j+3}$ (N $\cdot$ m^2) for $i, j = 1, 2, 3$.

Figure 4 shows the various material layups and the geometry of the CX-100 blade. Each color represents a section with unique material properties. Figure 5 shows the normalized bending stiffness along the length of the blade where a sharp gradient in the beam axial direction can be observed. The graph shows that the bending stiffness jumped to about 10% of its root value in under 10% of the blade length.

Figure 6 shows the test configuration for the static test performed at the National Wind Technology Center (NWTC) in Boulder, Colorado. The whiffle-tree configuration of the test apparatus applied the load at 3.00 m, 5.81 m, and 7.26 m from the root of the blade to achieve a maximum root moment of 128.6 kN m. The loads and positions are given in Table 4 below.

The out-of-plane displacements, u_3, at each of the load points were tracked for the experiment and are given in Table 5. The BeamDyn simulation was completed using four seventh-order LSFEs and the results are given in Table 5.

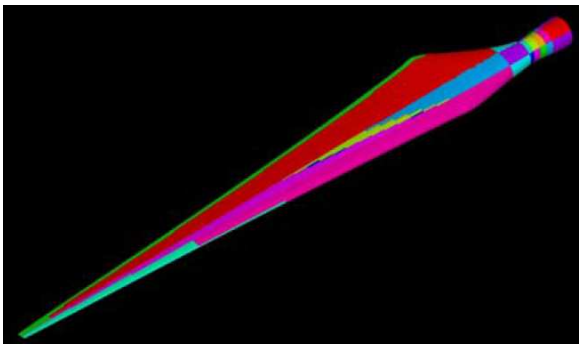

Figure 4: Material layup and geometry of the CX-100 wind turbine blade[21].

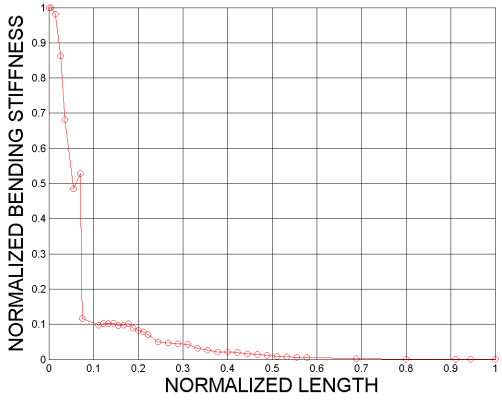

Figure 5: Normalized bending stiffness as a function of normalized blade length.

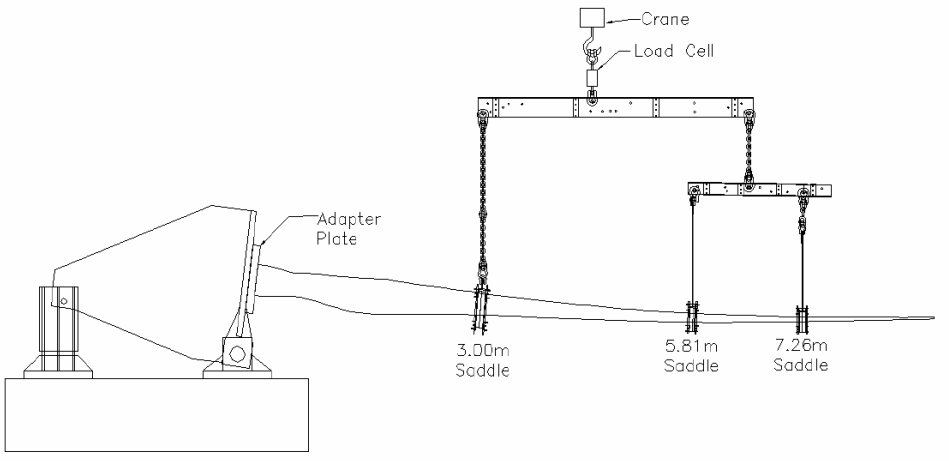

Figure 6: Test configuration for the static pull test conducted at the NWTC[21].

Table 4: Positions and applied loads during the CX-100 static loads testing at the NWTC

Saddle #	Radial Position (m)	Applied Load (kN)
1	3.00	16.9
2	5.81	5.47
3	7.26	5.59

Table 5: Experimental and BeamDyn simulation results for the CX-100 static test

	u_3 at saddle #1 (m)	u_3 at saddle #2 (m)	u_3 at saddle #3 (m)
Experimental	0.083530	0.381996	0.632460
BeamDyn	0.072056	0.381074	0.698850
Percent Error	13.74%	0.24%	10.5%

The displacements are plotted in Figure 7 and are overall in good agreement. One reason to explain the discrepancies between BeamDyn results and experimental data is that the coupling effects between the degrees of freedom was difficult to measure in the experiments. The results obtained by NLBeam, a nonlinear beam solver developed by Los Alamos National Laboratory, also can be found in Figure 7[22]. While the NLBeam solution was understood to use the same sectional data as the BeamDyn solution, it is currently unknown why the NLBeam solution differs. The focus of this case was to validate BeamDyn, not verify BeamDyn against NLBeam, and no attempt has been made to find the source of the differences.

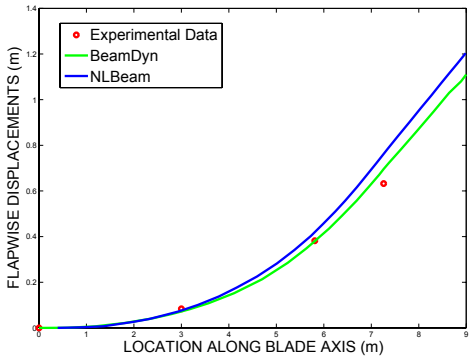

Figure 7: Displacement u_3 along the length of the blade for experimental data and BeamDyn simulation.

Next, a convergence study of the tip displacements was completed for the CX-100 blade in BeamDyn. Figure 8 shows the error as a function of the number of nodes (5 nodes represents 2 nodes per each of the 4 elements, 9 nodes represents 3 nodes per each of the 4 elements, etc.). The percentage error was calculated against the experimental data in Table 5. It can be seen that the convergence rate is not exponential as desired. This is likely due to the fact that as more nodes are added, different material-property stations are used; those data are not smoothly distributed in space. For the next simulation, the blade was meshed such that the element boundaries coincide with the locations where the sectional properties are defined. As previously mentioned, the cross-sectional properties for the CX-100 blade were given at 40 locations along the length of the blade. To have an element coincide with each sectional property, 39 LSFEs were needed. Figure 9 shows the results of this simulation. Each circle on the plot indicates an additional order of the LSFE, with the maximum being six. These results demonstrated that exponential convergence was achieved with this simulation, albeit with many elements. It can therefore be stated that for composite beams with sharp gradients and erratic data in the cross-sectional stiffness matrix, the spectral convergence is compromised, unless element boundaries coincident with the discontinuities. It should be noted here that although the convergence rate suffers as a result of sharp gradients and erratic data in the cross-sectional stiffness matrix as other finite element[22], the simulations still return reasonable results in comparison to the experiment data, suggesting that a lack of exponential convergence does not compromise the utility of BeamDyn.

C. Dynamics of a Cantilevered Beam

For verification of BeamDyn's dynamic analysis capability using the AM2 integrator, a benchmark problem for damping effects in the Dymore release package is used as an example. This example involves a dynamic analysis of a uniform cantilevered beam under an impulsive excitation, which is shown in Figure 10. The excitation was applied at the free tip along both the x_2 and x_3 directions simultaneously. The simulation range was 0 to 1 second. The sectional stiffness constants can be found in Table 6 and the units were the same as those used in the previous example. This beam is 2.4 meters long. The inertia properties were: 1.61 kg/m for the unit mass density, 8.60×10^{-4} and 1.10×10^{-4} kg m^2 for the mass moment of inertia about x_2 and x_3 direction, respectively. Two cases were analyzed: one without damping effects and the other with damping coefficients of 8.0×10^{-4} s for all the six degrees of freedom. The time

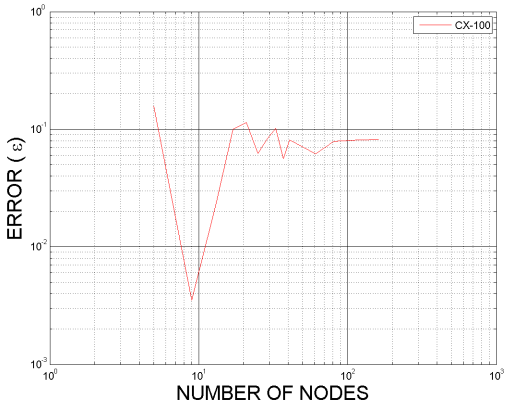

Figure 8: Percent error in u_3 as a function of the number of nodes.

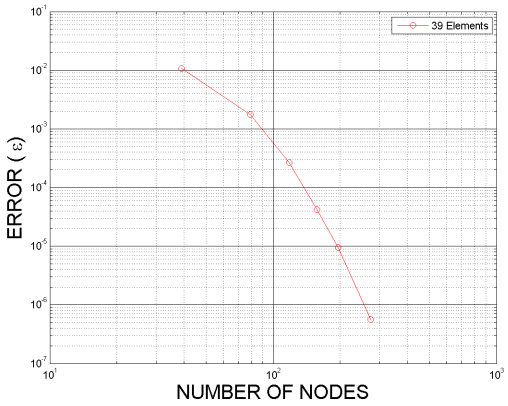

Figure 9: Percent error in u_3 compared to a highly refined solution in BeamDyn as a function of the number of nodes for 39 first- to sixth-order LSFEs, coincident with sectional properties.

steps for these two cases are 1×10^{-4} and 5×10^{-4} seconds, respectively, given that the damping will help the convergence and stability during simulation. The beam was discretized by one fifth-order element in BeamDyn analysis for a converged result. The time histories of all the displacement and rotation components are plotted in Figure 11. The damping effects can be clearly observed from these results. Furthermore, the accuracy of the present results of damped case were examined by the root-mean-square (RMS) errors, which aggregates the magnitudes of the errors in predictions for various times into a single measure of predictive performance. The error was calculated using

$$\varepsilon_{RMS} = \sqrt{\frac{\sum_{k=0}^{n_{max}} [u_3^k - u_b(t^k)]^2}{\sum_{k=0}^{n_{max}} [u_b(t^k)]^2}} \tag{48}$$

where $u_b(t)$ is the benchmark solution given by Dymore using eight third-order elements and 5×10^{-4}s time increment. The RMS error for three displacement components were 1.80×10^{-3}, 1.32×10^{-3}, and 2.70×10^{-3}, respectively.

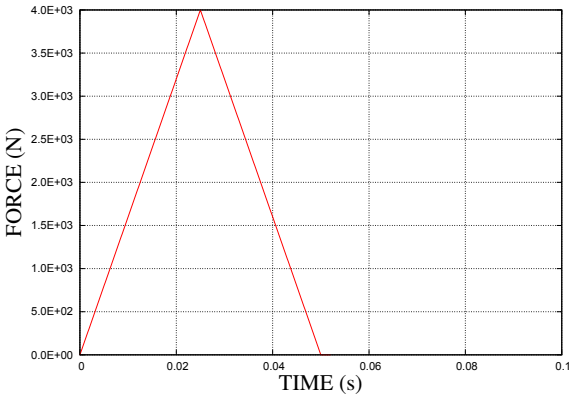

Figure 10: Impulsive excitation.

Table 6: Stiffness constants of the cantilevered beam in Example C

C_{11}	C_{22}	C_{33}	C_{44}	C_{55}	C_{66}
4.35E+07	1.40E+07	2.81E+06	2.81E+04	2.33E+04	2.99E+05

D. Analysis of NREL 5-MW Blade

The last example is to examine the efficiency and accuracy of the different time integrators that have been implemented in BeamDyn. The NREL 5-MW blade was analyzed in a cantilever condition, while a white-noise force is applied at the free tip along the flap direction. White noise was used to mimic the magnitude and frequency content of applied aerodynamic loads under realistic turbulent conditions. The damping coefficient is set to 10^{-3} s. Figure 12 shows the time history of the applied force and its power spectral density (PSD). The flap direction responses are plotted in Figure 13. Four cases were conducted in BeamDyn: the first three cases were using the AM2 time integrator with time step size: 2.5×10^{-2} s, 5×10^{-3} s, and 5×10^{-4} s, respectively, while the fourth case was using RK4 time integrator with time step sizes 5×10^{-6} s. It can be observed that for an implicit AM2 time step beyond 0.005 s, the solution is nearly identical to the fully resolved explicit RK4 solution. For an AM2 time step of 0.025 s, the solution remains stable and tracks the other solutions, but error grows at higher frequencies. The spikes at 0.7 Hz and 2 Hz correspond to the first and second blade flapwise natural frequencies, respectively. The spike above 5 Hz–above the frequency range of excitation–is brought about by nonlinear effects.

The convergence rate against time step size for the AM2 integrator is also examined. The result from the RK4 simulation is taken as the benchmark solution. The normalized RMS error defined in Eq. (48) is plotted in Figure 14, in which second-order convergence as a function of time increment size can be observed. It is also pointed out that a full Newton-Raphson algorithm has been implemented in BeamDyn. The total and average numbers of linear system solves, which are related to the computational time required for the solution, are plotted in Figure 15. It can be observed that while the total number of linear system solves reduces with increasing time step, the average number of solves per step increases. This means that the computation time cannot be cut in two by doubling the time step.

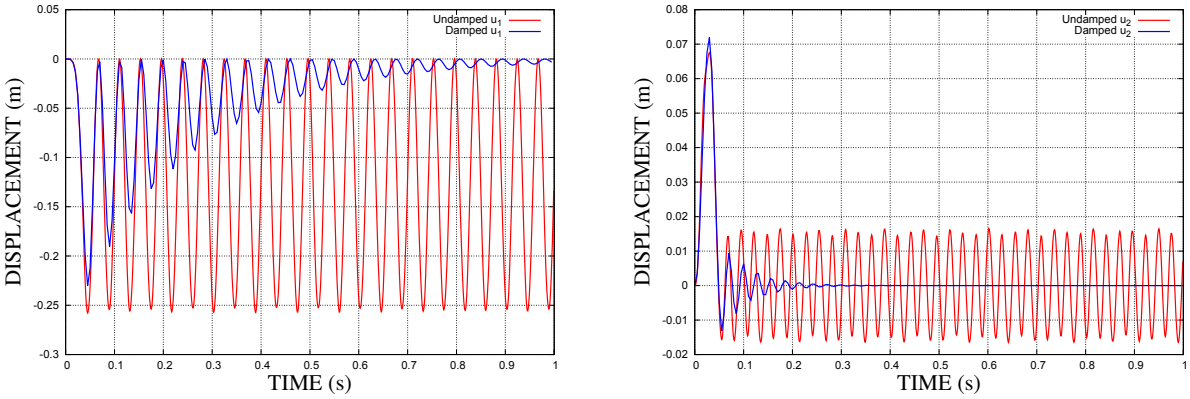

(a) u_1

(b) u_2

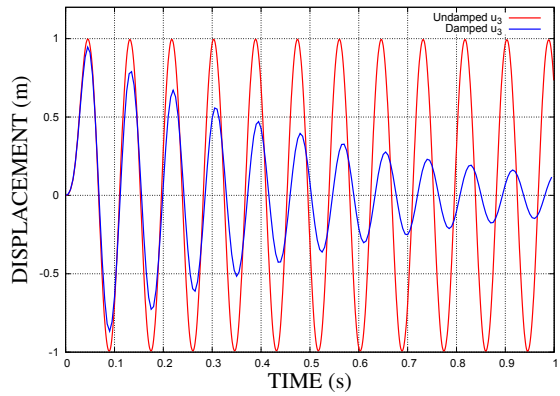

(c) u_3

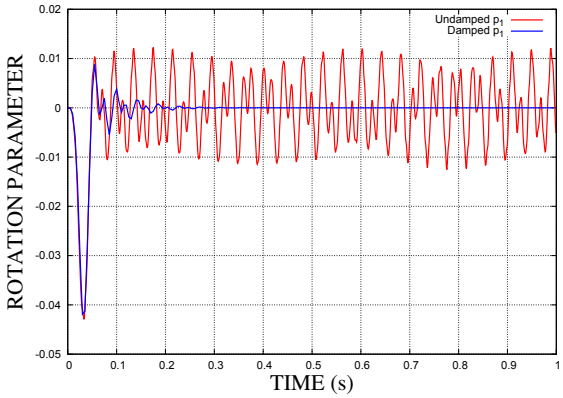

(d) p_1

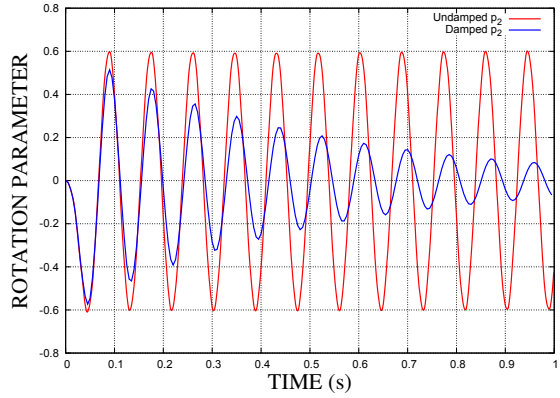

(e) p_2

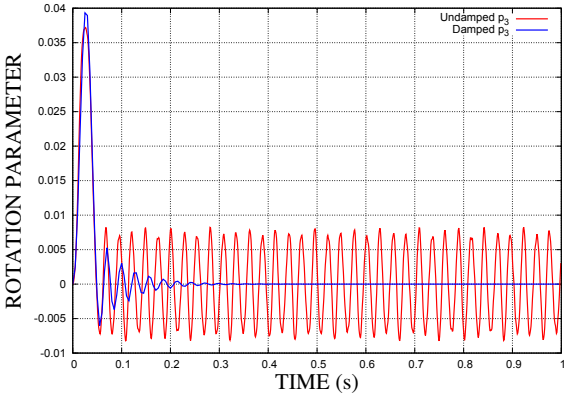

(f) p_3

Figure 11: Tip displacement and rotation histories of a cantilever beam under impulsive excitation.

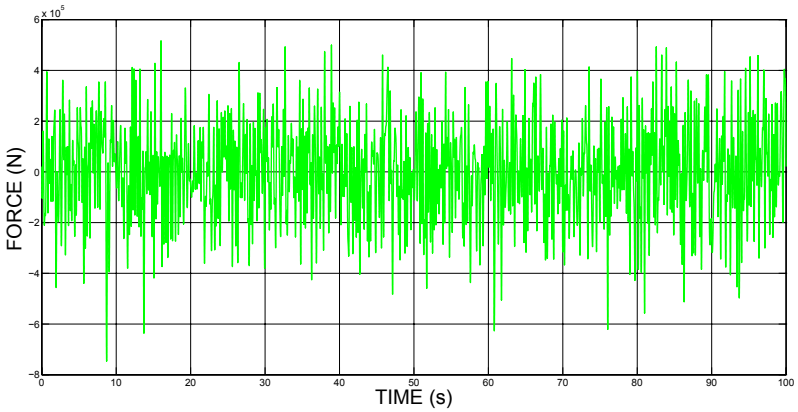

(a) Time history of applied force

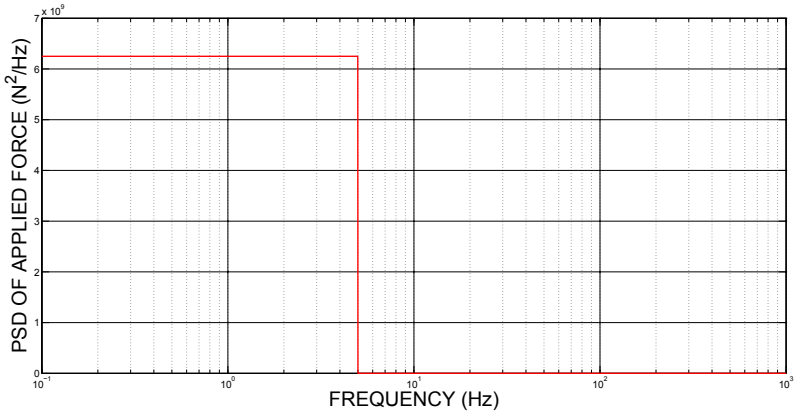

(b) PSD of applied force

Figure 12: Applied white noise force at the tip of a cantilevered NREL 5-MW blade.

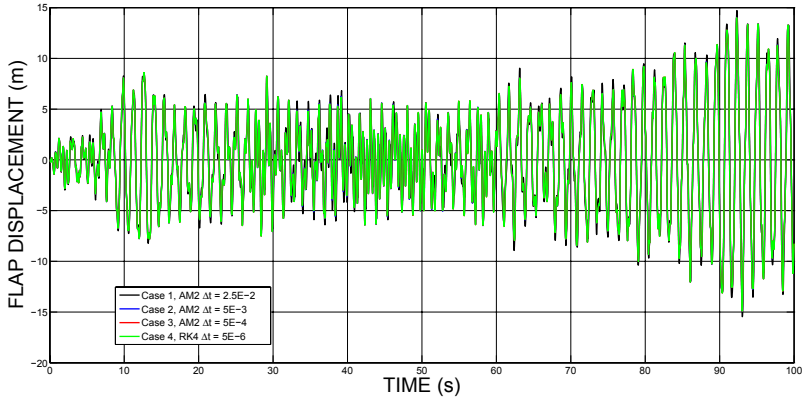

(a) Time history of flap displacement

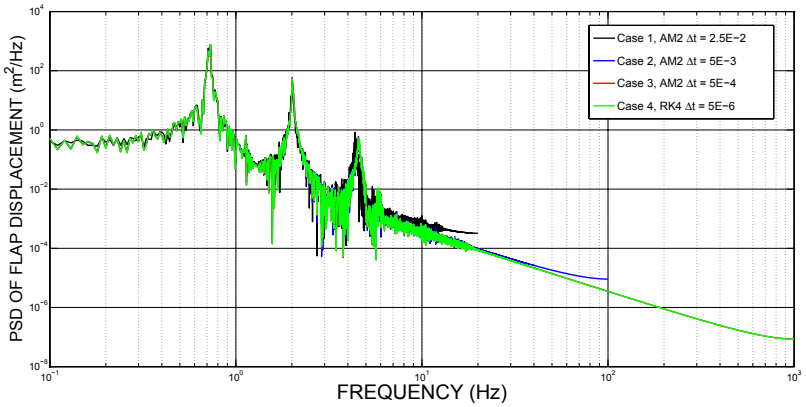

(b) PSD of flap displacement

Figure 13: Flap direction responses of a cantilevered NREL 5-MW blade under white noise excitation.

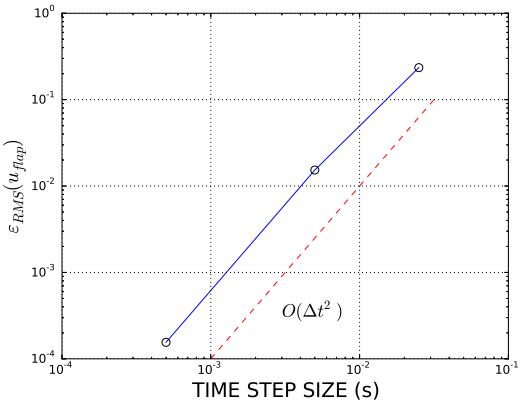

Figure 14: Normalized RMS error of flapwise displacement histories as a function of time step size for AM2 time integrator. The dashed line shows ideal second-order convergence.

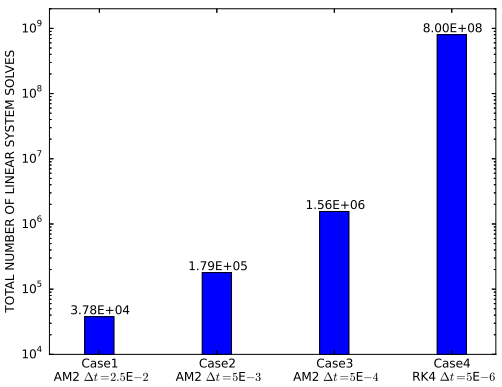

(a) Total number of linear system solves

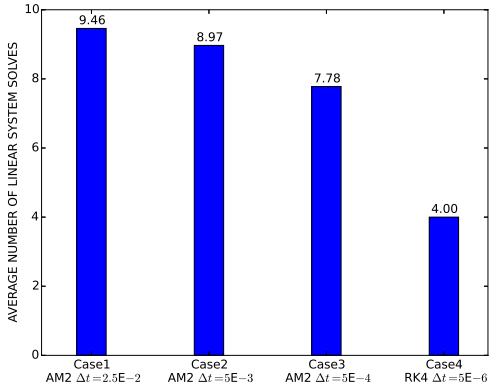

(b) Average number of linear system solves per step

Figure 15: Total and average numbers of linear system solves in the simulations.

VI. Summary

This paper reported on the development of BeamDyn, a beam solver in the FAST modularization framework. Geometrically exact beam theory has been reformulated into the first-order state-space form so that first-order time integrators, as required by FAST framework for tight-coupling analysis, can be applied. Numerical examples are provided to verify and validate the capability of BeamDyn in analyzing initially curved/twisted beams. A validation example is also presented where the numerical results are compared with experimental data. In all the cases, good agreement was observed. The convergence rate for analysis of realistic wind turbine blade is discussed. The features of BeamDyn can be summarized as follows:

1. Based on geometrically exact beam theory, BeamDyn is capable of dealing with geometric nonlinear beam problems with arbitrary magnitude of displacements and rotations for both static and dynamic analyses
2. Along with a preprocessor like PreComp or VABS, BeamDyn takes full elastic coupling effects into account
3. The governing equations are reformulated into state-space form, thus, making it amendable into FAST for tight-coupling analysis
4. The space is discretized by spectral finite elements, which is a p-version finite element, so that exponential convergence rate can be expected for smooth solutions
5. Different time integrators have been implemented in BeamDyn; users will have options based on their needs
6. BeamDyn is implemented following the programming requirements (data structures and interfaces) of the FAST modularization framework.

Future work includes the proposal of a practical approach to smooth the geometry and sectional constants to help achieve the expected exponential convergence rate. In addition, this module will be coupled to FAST and verification and validation will be conducted on a full wind turbine system.

Acknowledgments

This work was supported by the U.S. Department of Energy under Contract No. DE-AC36-08GO28308 with the National Renewable Energy Laboratory. Funding for the work was provided by the DOE Office of Energy Efficiency and Renewable Energy, Wind and Water Power Technologies Office. Support was also provided through a laboratory directed research and development grant *High-Fidelity Computational Modeling of Wind-Turbine Structural Dynamics*. The authors would also like to acknowledge D.J. Luscher for CX-100 sectional data.

References

[1]Reissner, E., "On one-dimensional large-displacement finite-strain beam theory," *Studies in Applied Mathematics LII*, 1973, pp. 87–95.

[2]Hodges, D. H., Saberi, H., and Ormiston, R. A., "Development of Nonlinear Beam Elements for Rotorcraft Comprehensive Analyses," *Journal of the American Helicopter Society*, Vol. 52, 2007, pp. 36–48.

[3]Simo, J. C., "A finite strain beam formulation. The three-dimensional dynamic problem. Part I," *Computer Methods in Applied Mechanics and Engineering*, Vol. 49, 1985, pp. 55–70.

[4]Simo, J. C. and Vu-Quoc, L., "A three-dimensional finite-strain rod model. Part II," *Computer Methods in Applied Mechanics and Engineering*, Vol. 58, 1986, pp. 79–116.

[5]Jelenić, G. and Crisfield, M. A., "Geometrically exact 3D beam theory: implementation of a strain-invariant finite element for statics and dynamics," *Computer Methods in Applied Mechanics and Engineering*, Vol. 171, 1999, pp. 141–171.

[6]Ibrahimbegović, A., "On finite element implementation of geometrically nonlinear Reissner's beam theory: three-dimensional curved beam elements," *Computer Methods in Applied Mechanics and Engineering*, Vol. 122, 1995, pp. 11–26.

[7]Ibrahimbegović, A. and Mikdad, M. A., "Finite rotations in dynamics of beams and implicit time-stepping schemes," *International Journal for Numerical Methods in Engineering*, Vol. 41, 1998, pp. 781–814.

[8]Hodges, D. H., *Nonlinear Composite Beam Theory*, AIAA, 2006.

[9]Yu, W. and Blair, M., "GEBT: A general-purpose nonlinear analysis tool for composite beams," *Composite Structures*, Vol. 94, 2012, pp. 2677–2689.

[10]Jonkman, J. M., "The new modularization framework for the FAST wind turbine CAE tool," *Proceedings of the 51st AIAA Aerospace Sciences Meeting including the New Horizons Forum and Aerospace Exposition*, Grapevine, Texas, January 2013.

[11]Jonkman, J. and Jonkman, B., "FAST v8," https://nwtc.nrel.gov/FAST8, October 2013, [Online; accessed 29-OCTOBER-2014].

[12]Wang, Q., Yu, W., and Sprague, M. A., "Gemoetrically nonlinear analysis of composite beams using Wiener-Milenković parameters," *Proceedings of the 54th Structures, Structural Dynamics, and Materials Conference*, Boston, Massachusetts, April 2013.

[13]Wang, Q. and Sprague, M. A., "A Legendre spectral finite element implementation of geometrically exact beam theory," *Proceedings of the 54th Structures, Structural Dynamics, and Materials Conference*, Boston, Massachusetts, April 2013.

[14]Wang, Q., Sprague, M. A., Jonkman, J., and Johnson, N., "Nonlinear Legendre spectral finite elements for wind turbine blade dynamics," *Proceedings of the 32nd ASME Wind Energy Symposium*, National Harbor, Maryland, January 2014.

[15]Sprague, M. A., Jonkman, J., and Jonkman, B., "FAST modular wind turbine CAE tool: non matching spatial and temporal meshes," *Proceedings of the 32nd ASME Wind Energy Symposium*, National Harbor, Maryland, January 2014.

[16]Bauchau, O. A., *Flexible Multibody Dynamics*, Springer, 2010.

[17]Gasmi, A., Sprague, M., and Jonkman, J., "Numerical stability and accuracy of temporally coupled multi physics modules in wind-turbine CAE tools," *Proceedings of the 51st AIAA Aerospace Sciences Meeting including the New Horizons Forum and Aerospace Exposition*, Grapevine, Texas, January 2013.

[18]Crisfield, M. and Jelenić, G., "Objectivity of strain measures in the geometrically exact three-dimensional beam theory and its finite-element implementation," *Proceedings of the Royal Society, London: Mathematical, Physical and Engineering Sciences*, Vol. 455, 1999, pp. 1125–1147.

[19]Bottasso, C. and Borri, M., "Integrating finite rotations," *Computer Methods in Applied Mechanics and Engineering*, Vol. 164, 1998, pp. 307–337.

[20]Bathe, K. J. and Bolourchi, S., "Large displacement analysis of three-dimensional beam structures," *International Journal for Numerical Methods in Engineering*, Vol. 14, 1979, pp. 961–986.

[21]Paquette, J., Lairdl, D., Griffith, D., and Rip, L., "Modeling and testing of 9m research blades," *44th AIAA Aerospace Sciences Meeting*, Vol. 19, 2006, pp. 14569–14581.

[22]Fleming, I. and Luscher, D. J., "A model for the structural dynamic response of the CX-100 wind turbine blade," *Wind Energy*, Vol. 17, 2013, pp. 877–900.